EDGE ARTICLE

Check for updates

All publication charges for this article have been paid for by the Royal Society of Chemistry

Mechanistic study of photocatalytic CO_2 reduction using a Ru(II)—Re(I) supramolecular photocatalyst†

Kei Kamogawa,[a] Yuushi Shimoda,[b] Kiyoshi Miyata,[b] Ken Onda,*[b] Yasuomi Yamazaki, ‡[a] Yusuke Tamaki[a] and Osamu Ishitani *[a]

Supramolecular photocatalysts comprising $[Ru(diimine)_3]^{2+}$ photosensitiser and *fac*-$[Re(diimine)(CO)_3\{OC(O)OC_2H_4NR_2\}]$ catalyst units can be used to reduce CO_2 to CO with high selectivity, durability and efficiency. In the presence of triethanolamine, the Re catalyst unit efficiently takes up CO_2 to form a carbonate ester complex, and then direct photocatalytic reduction of a low concentration of CO_2, *e.g.*, 10% CO_2, can be achieved using this type of supramolecular photocatalyst. In this work, the mechanism of the photocatalytic reduction of CO_2 was investigated applying such a supramolecular photocatalyst, **RuC2Re** with a carbonate ester ligand, using time-resolved visible and infrared spectroscopies and electrochemical methods. Using time-resolved spectroscopic measurements, the kinetics of the photochemical formation processes of the one-electron-reduced species **RuC2(Re)⁻**, which is an essential intermediate in the photocatalytic reaction, were clarified in detail and its electronic structure was elucidated. These studies also showed that **RuC2(Re)⁻** is stable for 10 ms in the reaction solution. Cyclic voltammograms measured at various scan rates besides temperature and kinetic analyses of **RuC2(Re)⁻** produced by steady-state irradiation indicated that the subsequent reaction of **RuC2(Re)⁻** proceeds with an observed first-order rate constant of approximately 1.8 s^{-1} at 298 K and is a unimolecular reaction, independent of the concentrations of both CO_2 and **RuC2(Re)⁻**.

Introduction

Currently, serious problems are being faced in terms of global warming, energy shortage and the dwindling of carbon resources. CO_2 reduction using sunlight, for its use as an energy source, is one of the useful photochemical reactions that can be utilised for producing energy and carbon resources to replace fossil fuels, leading to the suppression of CO_2 emission into the atmosphere.

Photocatalytic CO_2 reduction systems in which metal complexes are used both as photosensitizers and catalysts have been the subject of several research studies for approximately 40 years. Particularly, numerous studies have focused on *fac*-$[Re^I(diimine)(CO)_3L]^{n+}$-type complexes, which act as catalysts in various photocatalytic systems to selectively reduce CO_2 to CO with high efficiency.[1–4] Several of these photocatalytic systems are well known to work more efficiently in the presence of triethanolamine (TEOA), even when it does not act as a reductant and when a stronger reductant such as 1-benzyl-1,4-dihydronicotinamide or 1,3-dimethyl-2-phenyl-2,3-dihydro-1*H*-benzo[*d*]imidazole (BIH) is also present in the reaction solution. Although there have been several proposed reaction mechanisms for the photocatalytic reduction of CO_2 using this type of Re(I) complex as a photocatalyst or a catalyst,[4–8] the actual mechanism has not yet been elucidated. Particularly, a lack of information on the reactivity of the one-electron-reduced species (OERS) of Re complexes, which is produced as an essential intermediate in the photocatalytic reaction, is one of the reasons that has hindered further mechanistic investigation.

We previously reported that a TEOA adduct, *fac*-$[Re(diimine)(CO)_3(OC_2H_4NR_2)]$ (R = CH_2CH_2OH), in which deprotonated TEOA is ligated with an O^- atom, reacts with CO_2 dissolved in solution to give the corresponding carbonate ester complex, *fac*-$[Re(diimine)(CO)_3\{OC(O)OCH_2CH_2NR_2\}]$ (eqn (1)), which acts as the main catalyst in many photocatalytic CO_2 reduction reactions using *fac*-$[Re^I(diimine)(CO)_3L]^{n+}$-type complexes in the presence of TEOA.[9] A typical example of this is the photocatalytic CO_2 reduction using *fac*-Re(bpy)(CO)_3X (bpy = 2,2′-bipyridine; X = Br or Cl) as the sole metal complex in a reaction carried out in a mixed solvent of *N,N*-

aDepartment of Chemistry, Tokyo Institute of Technology, O-okayama 2-12-1, NE1, Meguro-ku, Tokyo 152-8550, Japan. E-mail: ishitani@chem.titech.ac.jp

bDepartment of Chemistry, Kyushu University, Fukuoka 819-0395, Japan. E-mail: konda@chem.kyushu-univ.jp

† Electronic supplementary information (ESI) available. See DOI: 10.1039/d1sc02213j

‡ Present address: Department of Materials and Life Science, Graduate School of Science and Engineering, Seikei University, 3-3-1 Kichijoji-kitamachi, Musashino-shi, Tokyo 180-8633, Japan.

dimethylformamide (DMF) and TEOA. This system was first reported by Lehn and co-workers[1] and is one of the most studied photocatalytic systems for CO_2 reduction.[4] It has been elucidated that in the initial stage of the photocatalytic reaction, fac-Re(bpy)$(CO)_3$X is converted to the corresponding carbonate ester complex fac-[Re(bpy)$(CO)_3$(OC(O)OCH$_2$CH$_2$NR$_2$)], which acts as the main catalyst but not as a photocatalyst.[9] It is also thought that the residual fac-Re(bpy)$(CO)_3$X acts as a redox photosensitizer to initiate photochemical electron transfer from TEOA to fac-[Re(bpy)$(CO)_3$(OC(O)OCH$_2$CH$_2$NR$_2$)]. However, the process behind the formation of the OERS of [Re(diimine)$(CO)_3$(OC(O)OCH$_2$CH$_2$NR$_2$)]-type complexes and their reactivities has not yet been reported. This reaction of the formation of a CO_2 adduct is an equilibrium reaction that has a very large equilibrium constant, $i.e.$, $K = $ [Re(bpy)$(CO)_3$(OC(O)OCH$_2$CH$_2$NR$_2$)]/[CO_2][Re(bpy)$(CO)_3$(OCH$_2$CH$_2$NR$_2$)] = 1.7×10^3 M^{-1} (eqn (1)).[9] Thus, this reaction in which CO_2 is captured can be applied for the photocatalytic and electrocatalytic reduction of low concentrations of CO_2.[10,11]

$$K = 1.7 \times 10^3 \text{ M}^{-1} \quad CO_2 \tag{1}$$
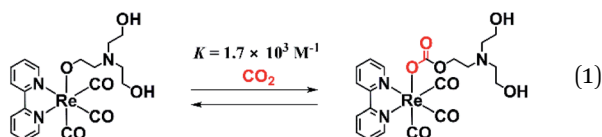
Recently, various supramolecular photocatalysts have been developed in which photosensitiser and catalyst units are connected to each other via a chemical bond.[12–14] Some of the reported Ru(II)–Re(I) supramolecular photocatalysts (for example **RuC2Re** in Scheme 1) have been reported to be more efficient photocatalysts compared with a mixed system involving Ru(II) photosensitiser and Re(I) catalyst mononuclear complexes (**Ru** and **Re**).[10,12,15–17] In photocatalytic CO_2 reduction reactions using supramolecular photocatalysts with various Re(I) catalyst units such as Re(diimine)$(CO)_3$Cl and [Re(diimine)$(CO)_2$\{P(p-F-C_6H_4)$_3$\}$_2$]$^+$, the CO_2 adduct of the Re(I) catalyst unit is also produced in the initial stage of the photocatalytic reaction, which acts as the actual photocatalyst in CO_2 reduction.[18,19] In a system using the supramolecular photocatalyst with a carbonate ester ligand the photocatalytic reduction of CO_2 proceeds efficiently in the Re catalyst unit even under a 10% CO_2 atmosphere, with a similar quantum yield (Φ) and turnover number (TON) for the formation of CO compared with the reaction carried out under a 100% CO_2 atmosphere. This type of supramolecular photocatalyst has recently been applied in various combined systems with solid materials, $e.g.$, Z-scheme-type photocatalysts with semiconductor materials that can induce the photocatalytic reduction of CO_2 using water as a reductant and only visible light as an energy source,[20] and in a light-harvesting photocatalyst based on a mesoporous organosilica material.[21]

Although fac-[Re(diimine)$(CO)_3$(OC(O)OCH$_2$CH$_2$NR$_2$)]-type complexes, including supramolecular photocatalysts, act as fascinating catalysts, several questions regarding their kinetics, thermodynamics, and mechanism in CO_2 reduction, such as the process behind the formation of the OERS and its reactivity,
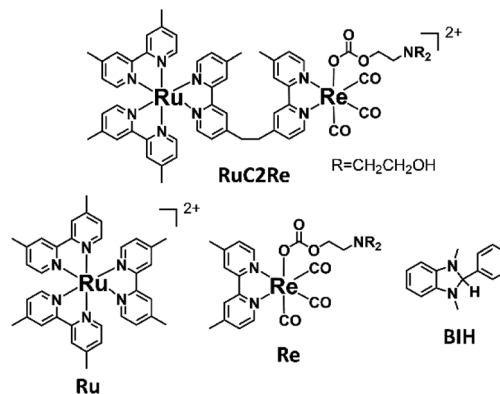
Scheme 1 Structures and abbreviations of the Ru(II)–Re(I) supramolecular photocatalyst and the model Ru(II) and Re(I) complexes, as well as the structure of BIH.

remain unanswered. Clarification of these questions is important in the development of more efficient and durable photocatalytic systems for CO_2 reduction.

In this study, the processes behind the formation of the OERS of **RuC2Re** and its reactivity using time-resolved infrared and visible (TR-IR and TR-vis) spectroscopy and electrochemical methods are examined.

Results and discussion

### Photocatalysis of RuC2Re for CO_2 reduction in DMSO–TEOA solution

To observe both the stretching bands of the CO ligands and the C=O group of the carbonate ester ligand in the supramolecular Ru(II)–Re(I) photocatalyst, when carrying out the Fourier-transform infrared (FT-IR) spectroscopic measurements, it is necessary to use a solvent that has a high transmittance in the absorption region of these vibrations, $i.e.$, between 1600 and 2100 cm^{-1}. N,N-Dimethylacetamide (DMA) and DMF containing TEOA mixed solutions, which have been commonly used in photocatalytic reactions involving Re(I) complexes as catalysts, barely transmit infrared light in some parts of this region. Thus, in this study, mixed dimethyl sulfoxide (DMSO)–TEOA (5 : 1 v/v) and DMSO–tetrahydrofuran (THF)–TEOA (5 : 5 : 2 v/v) solutions were used, the transmittances of which are good enough to allow FT-IR measurements to be carried out (Fig. S1 in the ESI†).
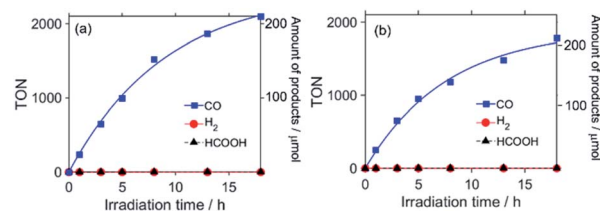
Fig. 1 Photocatalytic formation of CO (blue), H_2 (red), and formic acid (black) as a function of irradiation time. CO_2-saturated (a) DMSO–TEOA (5 : 1 v/v) and (b) DMSO–THF–TEOA (5 : 5 : 2 v/v) solutions containing **RuC2Re** (0.05 mM) and BIH (0.1 M) were irradiated at $\lambda_{ex} = $ 490–620 nm.

First, it was confirmed that **RuC2Re** exhibits sufficient photocatalytic activity in DMSO–TEOA solution. A CO_2-saturated DMSO–TEOA (5 : 1 v/v) solution containing **RuC2Re** (0.05 mM) and 1,3-dimethyl-2-phenyl-2,3-dihydro-1H-benzo[d]imidazole (BIH, 0.1 M) as a sacrificial electron donor was irradiated at λ_{ex} = 490–620 nm (λ_{ex}^{max} = 530 nm). Continuous and selective formation of CO was observed during the irradiation, as shown in Fig. 1a, with a very high turnover number (TON_{CO} = 2100) and selectivity (Γ_{CO} > 99%) of the formation of CO after 18 h of irradiation. The quantum yield of the production of CO (Φ_{CO}) was determined to be 40% using 480 nm monochromatic light with a light intensity of 5.0×10^{-9} einstein s^{-1} (Fig. S2†). These results show that **RuC2Re** efficiently reduces CO_2 to CO in DMSO–TEOA (5 : 1 v/v) with high selectivity and durability as well as in DMF–TEOA (5 : 1 v/v) and DMA–TEOA (5 : 1 v/v), which were used as solvents in previous studies.[1,2,10–20]

(2)

BIH   BIH•⁺   BI•   BI⁺
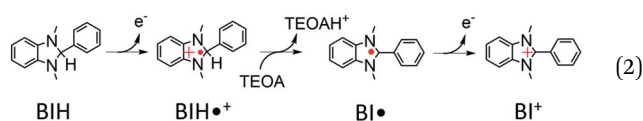
The photocatalytic reaction was monitored using $^{13}CO_2$ by measuring the ^1H and ^{13}C nuclear magnetic resonance (NMR) spectra before and after irradiation. A $^{13}CO_2$-saturated DMSO-d_6 solution containing TEOA (1.26 M), **RuC2Re** (0.14 mM), and BIH (0.1 M) was irradiated in an NMR tube at λ_{ex} = 490–620 nm (λ_{max} = 530 nm) for 22 h. In the ^1H NMR spectrum recorded before irradiation, peaks attributed to BIH (δ/ppm: 7.51–7.46 (m, 2H), 7.42–7.36 (m, 3H), 6.56 (dd, 2H, J = 5.5, 3.2 Hz), 6.38 (dd, 2H, J = 5.5, 3.2 Hz), 4.80 (s, 1H), and 2.42 (s, 6H)) were observed, but there were no peaks associated with its oxidised form (Fig. S3†). After the photocatalytic reaction, these peaks, which are related to BIH, decreased and new peaks that can be attributed to BI⁺ (δ/ppm: 8.06 (br, 2H), 7.88–7.68 (m, 7H), and 3.85 (s, 6H)) appeared. The concentrations of the reduced BIH and formed BI⁺, which is a two-electron oxidised and deprotonated compound of BIH (eqn (2)), are almost the same (0.086 M). In the ^{13}C NMR spectrum (nuclear Overhauser effect, NOE, complete ^1H-decoupling method) recorded after irradiation of the sample, peaks attributed to ^{13}CO (δ = 184.8 ppm) and $H^{13}CO_3^-$ (δ = 156.8 ppm), which were not observed before irradiation, were observed (Fig. S4†). The integral ratio of the $H^{13}CO_3^-$ peak against the peaks of TEOA (1.26 M) as an internal standard for the integration was 2.01 ± 0.05. The concentration of $H^{13}CO_3^-$ produced during the irradiation was calculated using this value and the natural abundance of ^{13}C in TEOA (1.07%), as shown in eqn (3).[22]

$$[H^{13}CO_3^-] = (2.01 \pm 0.05) \times [TEOA] \times 3 \times 0.0107$$
$$= 0.082 \pm 0.002 \text{ M} \quad (3)$$

Thus, the amount of reacted BIH was found to be almost equivalent to the amount of $H^{13}CO_3^-$ produced. As previously mentioned, ^{13}CO was detected in the ^{13}C NMR spectrum of the reaction solution after irradiation. In a similar experiment using ordinary CO_2 instead of $^{13}CO_2$, the ^{13}CO peak was not

observed. Note at this point that most of the produced CO should be released into the gas phase in the NMR tube because of the relatively low solubility of CO. Hence, these results clearly demonstrate that one molecule of CO_2 accepts two electrons from one molecule of BIH, with another CO_2 molecule serving as the final O^{2-} acceptor. Therefore, the overall reaction equation of the photocatalytic reaction using **RuC2Re** as a photocatalyst and BIH as a sacrificial electron donor in DMSO–TEOA is shown in eqn (4).

$$2CO_2 + BIH \rightarrow CO + HCO_3^- + BI^+ \quad (4)$$

Time-resolved spectroscopy

In the FT-IR spectrum of **RuC2Re** dissolved in DMSO–TEOA (5 : 1 v/v), recorded in an IR cell with an optical path length (d) of 0.2 mm, the stretching bands of the CO ligands can be clearly observed at 2018, 1911, and 1888 cm^{-1} and the C=O stretching band of the carbonate ester ligand can also be observed at 1668 cm^{-1} (Fig. S5†). However, because of the relatively low transmittance of the solvent in the range of 1600–1700 cm^{-1} and some technical issues that arose during the measurements,[23] the DMSO–TEOA (5 : 1 v/v) solvent was found to be not suitable for measuring the TR-IR spectra, for which an IR cell of d = 0.5 mm had to be used at these wavelengths. Hence, the solvent was diluted by adding THF, as it exhibits very high transmittance in the region of 1600–2100 cm^{-1}, to produce DMSO–THF–TEOA (5 : 5 : 2 v/v), which was then used as
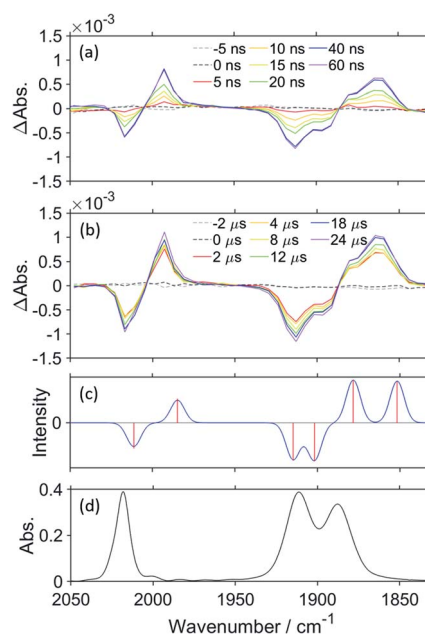
Fig. 2 TR-IR spectra measured at the indicated time delay after pulsed 532 nm excitation, (a) up to 60 ns and (b) up to 24 µs. A DMSO–TEOA (5 : 1 v/v) solution containing **RuC2Re** (0.2 mM) and BIH (0.1 M) was irradiated using 532 nm pump light (50 Hz) and probed (100 Hz). (c) DFT-calculated TR-IR spectrum of **Re⁻** (10 cm^{-1} Gaussian full width at half maximum (FWHM)). (d) FT-IR spectrum of **RuC2Re** (6 mM) in DMSO–TEOA (5 : 1 v/v); d = 0.2 mm.
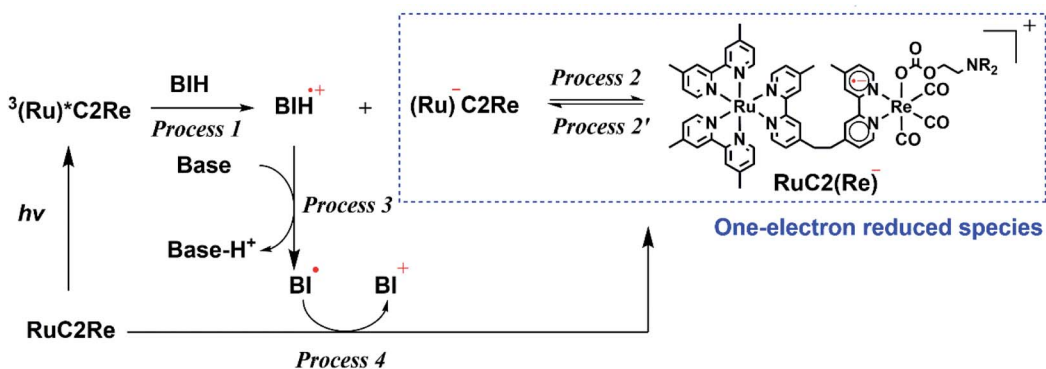
Scheme 2 Production processes of a one-electron-reduced species by BIH.

a solvent to carry out the TR-IR measurements in an IR cell of $d = 0.5$ mm. Fig. 1b shows the formation of the reduction products in the photocatalytic reaction using **RuC2Re** in DMSO–THF–TEOA (5 : 5 : 2 v/v), under the same conditions as shown in Fig. 1a, except for the use of the different solvents to give $TON_{CO} > 1800$ and $\Gamma_{CO} > 99\%$. This clearly indicates that **RuC2Re** is an efficient photocatalyst for CO_2 reduction, even in DMSO–THF–TEOA. Fig. S7c† and 4c show the FT-IR spectra of **RuC2Re** in DMSO–THF–TEOA (5 : 5 : 2 v/v). The stretching bands of the CO ligands can be observed at 2019, 1913, and 1890 cm^{-1}, besides the CO stretching band of the carbonate ester ligand at 1670 cm^{-1}. The absorption band at 1619 cm^{-1} can be attributed to the stretching bands of the diimine ligands of **Ru** and **Re**. It has already been reported that the spectra of *fac*-Re(diimine)(CO)$_3$-type complexes feature a diimine stretching band in this region.[24] Actually, the spectra of **Ru** and **Re** feature this band at 1619 and 1621 cm^{-1}, respectively (Fig. S6†). Notably, DMSO–TEOA (5 : 1 v/v) was mainly used as a solvent in the experiments to avoid concentration changes in the complex associated with CO_2 bubbling, which volatilises the THF in the DMSO–THF–TEOA solutions.

TR-IR measurements of CO_2-saturated reaction solutions containing **RuC2Re** and BIH were performed using the pump–probe method applying the second harmonic (532 nm) of a Nd:YVO$_4$ laser as the pump pulse. Fig. 2 and S7† display the TR-IR spectra in the region of the stretching vibrations of the CO ligands (1830–2050 cm^{-1}) in DMSO–TEOA (5 : 1 v/v) and DMSO–THF–TEOA (5 : 5 : 2 v/v), respectively, in which it can be observed that virtually the same results were obtained in both solvents. Two sets of negative bleaching bands ($\nu_{CO} = 2017$, 1913, and 1896 (sh) cm^{-1} in DMSO–TEOA; $\nu_{CO} = 2016$, 1912, and 1896 (sh) cm^{-1} in DMSO–THF–TEOA) and two sets of new absorption bands attributed to a reaction intermediate shifted ~25 cm^{-1} lower than the wavenumbers of the bleaching bands ($\nu_{CO} = 1993$, 1880 (sh), and 1865 cm^{-1} in DMSO–TEOA; $\nu_{CO} = 1992$, 1880 (sh), and 1864 cm^{-1} in DMSO–THF–TEOA) gradually appeared after the excitation. Bleaching bands were observed at similar wavenumbers to those of the ground state of **RuC2Re** (Fig. 2d and S7c†), which can be attributed to a decrease not only in the ground state of **RuC2Re** but also the excited state of the Ru unit (^{3}**(Ru)*C2Re**) and the OERS of the Ru unit

($($**Ru**$)^-$**C2Re**). As shown in Scheme 2 these three states have similar ν_{CO} bands because of the weak interaction between the Ru and the Re units of this binuclear complex.[25,26] These changes in the TR-IR spectra proceed *via* two steps, a fast process (Fig. 2a and S7a†) and a subsequent slower process (Fig. 2b and S7b†). The fast process proceeded for several of tens of nanoseconds after the excitation, which can be attributed to the production of **RuC2(Re)**$^-$ *via* reductive quenching of the excited state of the Ru unit (*Process 1* shown in Scheme 2) followed by fast intramolecular electron transfer to the Re unit (*Process 2* shown in Scheme 2). In the photocatalytic reduction of CO_2 using **RuC2Re** and BIH in DMF–TEOA solution, we previously reported that BIH$^{•+}$ produced in *Process 1* is deprotonated and converts to BI$^•$ (*Process 3* shown in Scheme 2), which has a strong reducing power ($E^p_{ox} = -1.93$ V *vs.* Ag/AgNO$_3$ (-2.11 *vs.* Fc$^{+/0}$)).[16] Therefore, the slower process, which proceeded up to several microseconds in the DMSO–TEOA and DMSO–THF–TEOA solutions, can also be attributed to the reduction of ground state **RuC2Re** by BI$^•$ (*Process 4* shown in Scheme 2). The UV-vis absorption spectra of **Ru**, **Re**, and **RuC2Re** shown in Fig. 3 clearly indicate that the intramolecular electronic interaction between the Ru and Re units is weak in the ground state as the **RuC2Re** spectrum can be well simulated *via* the summation of the **Ru** and **Re** spectra. Since the driving force of intramolecular electron transfer from the reduced Ru unit to the Re unit is estimated to be $\Delta G_{et} = -30$ meV,
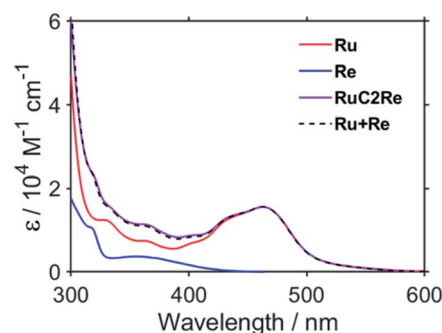

Fig. 3 UV-vis absorption spectra of **Ru** (red), **Re** (blue), and **RuC2Re** (purple). The fitting result is shown as a dashed black line.
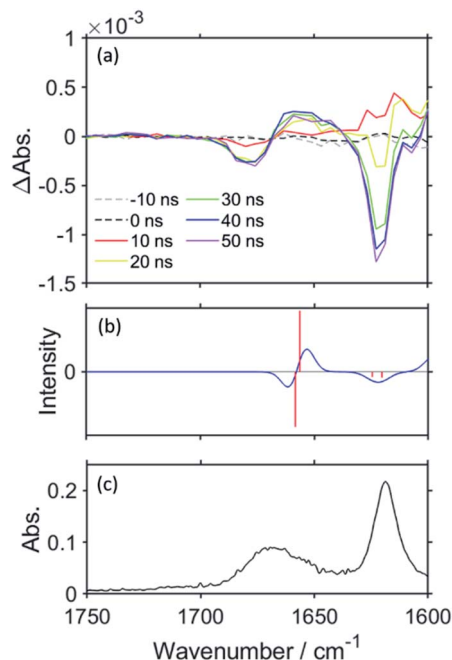
Fig. 4 (a) TR-IR spectra measured at the indicated time delay after pulsed 532 nm excitation. A DMSO–THF–TEOA (5 : 5 : 2 v/v) solution containing **RuC2Re** (1.0 mM) and BIH (0.1 M) was irradiated with 532 nm pump light (50 Hz) and probed (100 Hz). (b) DFT-calculated TR-IR spectrum of **Re**$^-$ (10 cm^{-1} Gaussian FWHM; scaling factor = 0.965). (c) FT-IR spectrum of **RuC2Re** (3 mM) in DMSO–THF–TEOA (5 : 5 : 2 v/v); d = 0.5 mm.

calculated from the difference between the first redox potentials of **Ru** (E(**Ru**/**Ru**$^-$) = −1.63 V *vs.* Ag/AgNO$_3$ (−1.81 V *vs.* Fc$^{+/0}$)) and **Re** (E(**Re**/**Re**$^-$) = −1.60 V *vs.* Ag/AgNO$_3$ (−1.78 V *vs.* Fc$^{+/0}$)) (Fig. S8† and 9(b)), the electron transfer from the OER Ru unit to the Re unit is slightly exergonic, and this intramolecular electron transfer should be reversible. These electron transfer reactions, which proceed *via* a through-bond mechanism, should be sufficiently faster than *Process 4*, *i.e.*, the reduction of **RuC2Re** in its ground state by BI˙, and pseudo-equilibrium between (**Ru**)$^-$**C2Re** and **RuC2(Re)**$^-$ was achieved within 60 ns (end of *Process 1*, Scheme 2) when the forward and reverse electron transfer rates became equal.[25,26]

Fig. 4a shows the TR-IR spectra of **RuC2Re** in the region of ν_{CO} of the carbonate ester ligand and the diimine ligand vibrations (1600–1750 cm^{-1}) measured in DMSO–THF–TEOA. Two negative bands can be observed in the spectra at 1676 and 1622 cm^{-1} after the excitation, which can be attributed to the ν_{CO} of the carbonate ester ligand and the diimine ligands of

RuC2Re, where the bleaching band of ν_{CO} (1676 cm^{-1}) is shifted to a higher wavenumber compared with ν_{CO} (1670 cm^{-1}, Fig. 4c), which indicates partial overlap of this negative peak with the positive band attributed to the ν_{CO} of the carbonate ester ligand of **RuC2(Re)**$^-$, which forms on this timescale. As the reduction of the Re unit increases the electron density on the π^* orbital of the carbonate ester ligand, it is predicted that the ν_{CO} of the carbonate ester ligand of **RuC2(Re)**$^-$ should shift to a lower wavenumber compared to that of **RuC2Re**. It can be expected that the overlap of the ν_{CO} bands of **RuC2Re** and **RuC2(Re)**$^-$ is a result of this small shift. Under the assumption that the shapes of the ν_{CO} absorption bands of the carbonate ester ligands of **RuC2Re** and **RuC2(Re)**$^-$ are the same, the 1630–1700 cm^{-1} region of the TR-IR spectrum was fitted using the FT-IR spectrum of **RuC2Re**, from which the ν_{CO} of the carbonate ester ligand of **RuC2(Re)**$^-$ was estimated to be 1664 cm^{-1} (Fig. S9†). This indicates that the ν_{CO} shift of the carbonate ester ligand caused by the OERS of the Re unit is only 6 cm^{-1} and is much smaller than that of the CO ligands (24 cm^{-1}). These spectral results strongly suggest that the structure of the carbonate ester ligand of **RuC2(Re)**$^-$ is retained and that the additional electron is mainly localised on the diimine ligand in the Re unit. The corresponding positive band to the bleaching band at 1622 cm^{-1} cannot be observed between 1600 and 2100 cm^{-1}, which should be red-shifted because of the increase in the electron density on the π^* orbital of the diimine ligand(s).

Density functional theory (DFT) was applied to support the assignment of the peaks of **RuC2(Re)**$^-$ observed in the TR-IR spectra. As the electronic interaction between the Ru and Re units is weak as described above, DFT calculations were performed for a model mononuclear complex of the Re unit, *i.e.*, **Re** and its OERS **Re**$^-$, to simplify the calculations. Fig. 2c and 4b show the calculated IR spectra, which are in good agreement with the TR-IR spectra, as can be observed in the data presented in Table 1. The singly occupied molecular orbital (SOMO) of **Re**$^-$ is mainly distributed on the diimine ligand (Fig. S10†). Mulliken analysis was performed to examine the difference in charge density between **Re** and **Re**$^-$ in more detail, with the results presented in Table S1.† The data obtained show that the most negatively charged ligand is the diimine. However, the charge densities at the carbonate ester bonds of **Re** and **Re**$^-$ are very similar, which is consistent with the slight shift in the ν_{CO} band of the carbonate ester ligand, and strongly supports the distribution of the added electron in **RuC2(Re)**$^-$ as described above. It is noteworthy that, because of the flexibility of the carbonate ester ligand, there are several possible stable

Table 1 IR stretching frequencies of **RuC2Re** in DMSO–THF–TE0A (5 : 5 : 2 v/v) and DFT-calculated gas phase **Re**

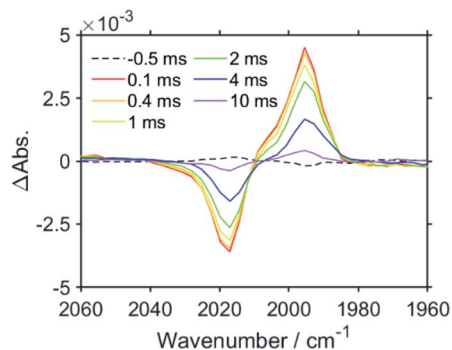|	Calculated ν_{CO} (cm^{-1}) of **Re**	Experimental ν_{CO} (cm^{-1}) of **RuC2Re**
Nonreduced state	2011, 1915, 1902 (CO ligands)	2019, 1913, 1890
	1658 (carbonate ester)	1670
One-electron-reduced state	1985, 1878, 1852 (CO ligands)	1992, 1880 (sh), 1864
	1656 (carbonate ester)	1664 (fitting result)

Fig. 5 TR-IR spectra measured at the indicated time delay after pulsed 526 nm excitation. A DMSO–TEOA (5 : 1 v/v) solution containing **RuC2Re** (0.2 mM) and BIH (0.1 M) was irradiated using 526 nm pump light (25 Hz) and probed (50 Hz).

structures of **Re** and **Re⁻**, with the calculations for all of the structures giving similar results, as shown in Fig. S11 and Table S2.†

Fig. 5 shows the TR-IR spectra measured on a longer time-scale, *i.e.*, up to 10 ms after excitation. It is noteworthy that, even after 10 ms, the ν_{CO} bands of the CO ligands do not change, although there is a gradual decrease in the intensities of the bleaching and positive bands. This decay in the bands is thought to be caused by the diffusion of the reduced species to the out of the probe light region due to the flow of the solution and/or the oxidation of the OERS by contaminated O₂. These results strongly indicate that **RuC2(Re)⁻** is stable up to 10 ms, even under an atmosphere of CO₂.

Fig. 6 shows the TR-vis absorption of a CO₂ saturated DMSO–TEOA (5 : 1 v/v) solution containing **RuC2Re** and BIH measured using the randomly interleaved pulse train (RIPT) method applying the second harmonic (532 nm) of a Nd:YAG laser as the pump pulse.[27] After the excitation, the absorption band at λ_{max} = 519 nm was observed to increase in intensity. Although the broad absorption band at >580 nm also initially increased in intensity, it started to decrease in intensity 5 μs after the excitation (Fig. 6a). The absorption changes at 519 and 621 nm are

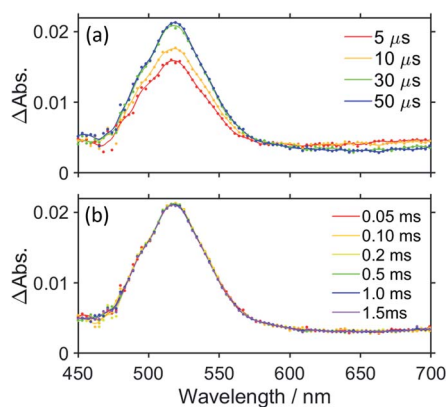**Fig. 6** TR-vis spectra at the indicated time delay recorded after 532 nm excitation of **RuC2Re** (0.2 mM) in a CO₂-saturated DMSO–TEOA (5 : 1 v/v) solution containing BIH (0.1 M): (a) up to 50 μs and (b) up to 1.5 ms.

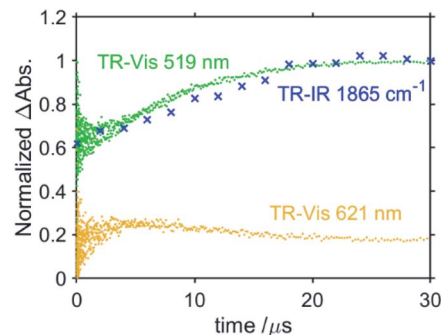**Fig. 7** Temporal changes in Δ_{Abs} at 519 and 621 nm (TR-vis, green and orange), and 1865 cm⁻¹ (TR-IR, blue), normalised at 30 μs.

shown in the spectrum in Fig. 7, in which the TR-IR behaviour of the absorbance at 1865 cm⁻¹ of **RuC2(Re)⁻** can also be observed (Fig. 2b). The absorption at 519 nm was observed to increase in intensity immediately after excitation and then more slowly up to 30 μs, which corresponds to the temporal behaviour of the absorption at 1865 cm⁻¹. Since the feature of the absorption band at λ_{max} = 519 nm is similar to the previously reported results for the OERS of other Ru(ɪɪ)–Re(ɪ) supramolecular photocatalysts, it can be attributed to the absorption band of **(Ru)⁻C2Re** and **RuC2(Re)⁻**, of which the Ru unit or the Re unit is respectively reduced to its one-electron-reduced form.[12,28] As the intramolecular electron transfers between the Ru and Re units of the OERS of **RuC2Re** (*Processes 2* and *2′* in Scheme 2) proceed on the nanosecond timescale as described above, the equilibrium between them should be quickly reached and, afterward, the ratio between **(Ru)⁻C2Re** and **RuC2(Re)⁻** should not change. Although the ratio between **(Ru)⁻C2Re** and **RuC2(Re)⁻** could not be determined because of the molar extinction coefficients of the OERS of the Re unit not being known, it is thought that the [**RuC2(Re)⁻**]/[**(Ru)⁻C2Re**] ratio is greater than 1 because of the following reasons: (1) the shape of the absorption band is quite different from that of the OERS of **Ru** (**Ru⁻**) (Fig. S12†) and (2) the first reduction potential of **Re** ($E_{1/2}$ = −1.60 V *vs.* Ag/AgNO₃ (−1.78 V *vs.* Fc⁺/⁰) which is described in detail below) is more positive than that of **Ru** ($E_{1/2}$ = −1.63 V *vs.* Ag/AgNO₃ (−1.81 V *vs.* Fc⁺/⁰)). The slow increase in the growth of the absorption band at λ_{max} = 519 nm can be attributed to another formation process of the OERS of **RuC2Re**, to which the electron donor is BI·, because of the similarity in the timescale of the growth of the TR-IR absorption band at 1865 cm⁻¹ attributed to **RuC2(Re)⁻** (Fig. 2b). Another absorption band at 621 nm was observed to grow for up to 5 μs after the excitation and then decreased as described above. This decay was observed to proceed on the same timescale as the second-step increase at 519 nm. The TD-DFT calculations in Fig. S13† show that this broadband can be attributed to BI·, which is produced in *Process 3*, as shown in Scheme 2. The decay of this band proceeds on the same timescale as the slower growth of the absorption band at λ_{max} = 519 nm, which validates *Process 4* shown in Scheme 2, *i.e.*, that the reduction of **RuC2Re** in the ground state by BI· proceeds on this timescale.

Fig. 6b shows the TR-vis spectra measured on a longer timescale, *i.e.*, up to 1.5 ms after excitation. The spectra show that the shape of the absorption band of the OERS of **RuC2Re** does not change between 50 μs and 1.5 ms after laser excitation, which means that the OERS of **RuC2Re**, *i.e.*, $(\mathbf{Ru})^-$**C2Re** and **RuC2(Re)**$^-$, are stable on this timescale. This is consistent with the experimental TR-IR results.

UV-vis absorption spectral changes during and after steady-state irradiation

To elucidate the kinetics of the subsequent reaction of the one-electron-reduced Re unit, the following experiments were performed. A CO_2-saturated DMSO–TEOA (5 : 1 v/v) solution containing **RuC2Re** (0.05 mM) and BIH (0.1 M) was irradiated under a 500 W xenon (Xe) arc lamp fitted with a bandpass filter at 2.6×10^{-8} einstein s^{-1} using strong steady-state light at 480 nm, much higher light intensity than that used in the photocatalytic reactions (see Fig. S2,† for example), and visible absorption spectral changes were measured during and after the irradiation. Fig. 8a shows the spectral changes that take place during the irradiation, in which a broad absorption band appears at $\lambda_{\max} = 515$ nm, which can be attributed to a mixture of $(\mathbf{Ru})^-$**C2Re** and **RuC2(Re)**$^-$ according to similarity to the TR-vis results, shown in Fig. 6. This result indicates that the rate of production of the OERS is faster than the rate of the subsequent reaction of the OERS over this time period. The rate of accumulation of the OERS can be seen to decrease in line with the irradiation time. This is because the subsequent reaction is accelerated by the increase in the concentration of the OERS. When the irradiation was continued for 1.7 s and then stopped, the absorption band of the accumulated OERS began to decrease, as shown in Fig. 8b. Fig. 8c shows the temporal changes in Δ_{Abs} at 519 nm, of which the decay curve can be well fitted using a single exponential function, where the observed first-order rate constant is $k_{\mathrm{obs}} = 1.8 \pm 0.1$ s^{-1}. We performed this experiment four times to determine the error in k_{obs}. Since, in this experiment, the steady-state light was irradiated from only one direction and the solution was not stirred during the

reaction, the reaction solution should reflect the concentration gradient of the OERS. To evaluate the effect that diffusion has on the concentration gradient, the same experiment was carried out, except that **Ru** was used instead of **RuC2Re**, the OERS (**Ru**$^-$) of which is stable on this timescale. In this process, an argon-saturated DMSO–TEOA (5 : 1 v/v) solution containing **Ru** (0.05 mM) and BIH (0.1 M) was irradiated at 480 nm (5.3×10^{-9} einstein s^{-1}) to accumulate **Ru**$^-$ (Fig. S14a†). Although the absorption band of the accumulated **Ru**$^-$ slowly decayed after the irradiation was stopped because of diffusion (Fig. S14b†), the rate of decay was approximately 37 times slower than that of the OERS of **RuC2Re**, as shown in Fig. 8c. Since the charges of the OERSs of **RuC2Re** and **Ru** are the same and the molecular radius of the OERS of **RuC2Re** is larger than that of **Ru**, the diffusion of the OERS of **RuC2Re** *via* a concentration gradient should be slower than that of **Ru**. Thus, the effect of diffusion is almost negligible when evaluating the rate constant of the subsequent reaction of **RuC2(Re)**$^-$, which is $k = 1.8$ s^{-1}. Note that this decay can be fitted using a first-order kinetics model but not using a second-order model. Hence, the disproportionation of the OERS of **RuC2Re** does not proceed as the main process of the subsequent reaction(s) of the OERS of **RuC2Re**.

Electrochemistry

To examine the subsequent reaction of the one-electron-reduced Re unit in more detail, cyclic voltammograms (CVs) of **Re** as a model of the Re unit of **RuC2Re** were recorded at various scan rates in a CO_2-saturated DMSO–TEOA (5 : 1 v/v) solution containing **Re** (1 or 2 mM) and tetraethylammonium tetrafluoroborate (Et_4NBF_4, 0.1 M) as a supporting electrolyte. At slow scan rates, *e.g.*, 200 mV s^{-1} (Fig. 9a), an irreversible one-electron reduction wave at $E_{\mathrm{p}} = -1.66$ V *vs.* Ag/AgNO$_3$ (-1.84 V *vs.* Fc$^{+/0}$) and a catalytic wave at $E_{\mathrm{p}}^{\mathrm{cat}} = -2.00$ V (-2.18 V *vs.* Fc$^{+/0}$) are observed. Fig. S15† shows the dependence of the scan rate on the first one-electron reduction wave of the process at $E_{\mathrm{p}} = -1.66$ V *vs.* Ag/AgNO$_3$ (-1.84 V *vs.* Fc$^{+/0}$), in which it can be seen that upon increasing the scan rate, the process becomes more reversible. At 30 V s^{-1} using an ultra-micro glassy carbon working electrode, the first reduction wave is reversible and the $E_{1/2}^{\mathrm{red}}$ is -1.60 V *vs.* Ag/AgNO$_3$ (-1.78 V *vs.* Fc$^{+/0}$) (Fig. 9b). These
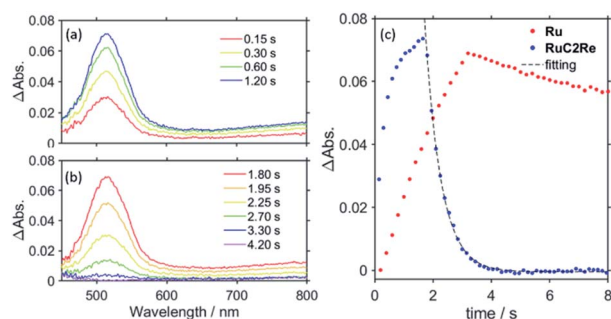

Fig. 8 (a) Visible differential absorption spectra of **RuC2Re** (0.05 mM) in a CO_2-saturated DMSO–TEOA (5 : 1 v/v) solution containing BIH (0.1 M) during irradiation at 480 nm (2.6×10^{-8} einstein s^{-1}) (b) and after irradiation. (c) Temporal changes in Δ_{Abs} at $\lambda = 519$ nm of **RuC2Re** (blue) and **Ru** (red, see Fig. S14 in the ESI†) during and after the irradiation.
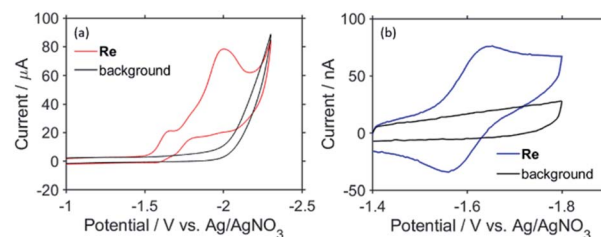

Fig. 9 (a) CV of **Re** (2 mM) in a CO_2-saturated DMSO–TEOA mixed solution; WE: glassy carbon (diameter = 3 mm), RE: 0.01 mM Ag/AgNO$_3$, CE: Pt wire, supporting electrolyte: 0.1 M Et_4NBF_4 (0.1 M), scan rate: 200 mV s^{-1}, $T = 298$ K. (b) CV of **Re** measured in a DMSO–TEOA (5 : 1 v/v) solution under a CO_2 atmosphere; WE: glassy carbon ultra-micro electrode (diameter = 33 μm), RE: 0.01 mM Ag/AgNO$_3$, CE: Pt wire, supporting electrolyte: Et_4NBF_4 (0.1 M), scan rate: 30 V s^{-1}.

results indicate that the subsequent chemical reaction of the OERS of **Re**, *i.e.*, **Re⁻**, should proceed on the timescale of the CV experiments. Thus, the CVs of **Re** were fitted *via* digital simulation using an ALS/CHI620EX electrochemical analyser under the assumption that the process proceeds *via* an EC mechanism, as shown in eqn (5) and (6), where the background currents were subtracted from the CVs before the fitting. The fittings of the CVs were found to be reasonable, as shown in Fig. 10, with the rate constant of the chemical reaction of **Re⁻** (k_c) determined as 2.1 s⁻¹.

$$Re + e^- \rightleftharpoons Re^- \quad (5)$$

$$Re^- \xrightarrow{k_c} Intermediate \quad (6)$$
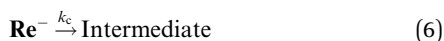
Note that if the reduction potential of the intermediate produced by the subsequent reaction of **Re⁻** (eqn (6)) is close to or more positive than −1.60 V, the value of k_c may be overestimated from its actual value because this intermediate is also reduced on the electrode, *i.e.*, *via* an ECE mechanism; however, it does not induce a large difference in the value of k_c. The calculated value is actually close to the experimental result using the steady-state light described above ($k = 1.8$ s⁻¹). Also note that the k_c value is not dependent on the concentration of **Re** in the solution. Additionally, both the reversibility of the first reduction wave and the value of k_c are independent of the concentration of CO_2 in the solution (Fig. S16†). Hence, CO_2 is not involved in the subsequent reaction of **Re⁻**, and the disproportionation of the two molecules of **Re⁻** is also omitted from possible processes in CO_2 reduction.

The first reduction wave of **Re** becomes more irreversible at a higher temperature, which indicates that the subsequent

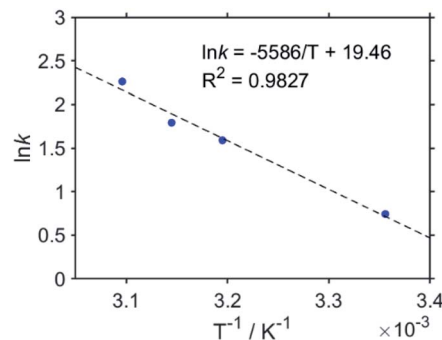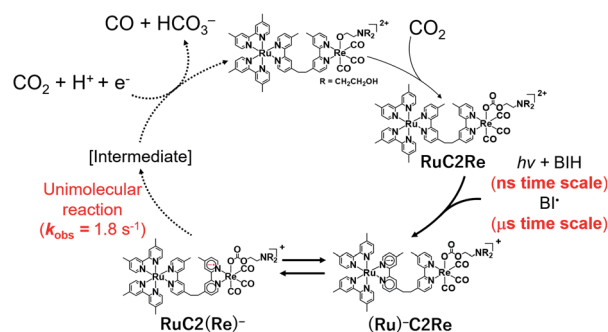Fig. 11 Arrhenius plot from which k_c is derived.

Fig. 12 Proposed mechanism of CO_2 reduction using **RuC2Re**.

reaction of **Re⁻** is accelerated (Fig. S17†). Good linear Arrhenius plots were obtained, as shown in Fig. 11, and the activation energy of the subsequent reaction of **Re⁻** was obtained as $E_a = 46$ kJ mol⁻¹. The results of the electrochemical measurements of **Re** can be summarised as follows. The lifetime of **Re⁻** was calculated to be ∼500 ms. Neither the disproportionation of **Re⁻** nor a bimolecular reaction between **Re⁻** and CO_2 proceeds in the subsequent reaction of **Re⁻**. In other words, **Re⁻** reacts according to first-order kinetics, with an activation energy of $E_a = 46$ kJ mol⁻¹. Note that the chemical properties of **Re⁻** and the reduced Re unit of **RuC2(Re)⁻** are similar to each other because of the weak interactions between the Ru and the Re units in **RuC2Re**. These results indicate that the subsequent reaction of **RuC2(Re)⁻** is a unimolecular reaction, such as the structural change of the reduced Re unit (Fig. 12).

Although we do not have conclusive evidence about the following processes including the structure of the intermediate produced by the unimolecular process of the one-electron reduced Re unit in **RuC2(Re)⁻**, we can presume a possible mechanism based on our experimental results and previously reported information as follows. Recombination of the carbonate ester ligand, *i.e.*, change of the Re–O bond to a Re–C bond, followed by dissociation of a C–O bond gives the corresponding carboxylate Re complex [(diimine)(CO)₃Re–C(O)OR] (R = $C_2H_4N(CH_2CH_2OH)_2$ or H). Reduction of this complex might induce elimination of CO from the carboxylate ligand of the metal complex, which has been proposed in some photocatalytic and electrocatalytic CO_2 reduction reactions using
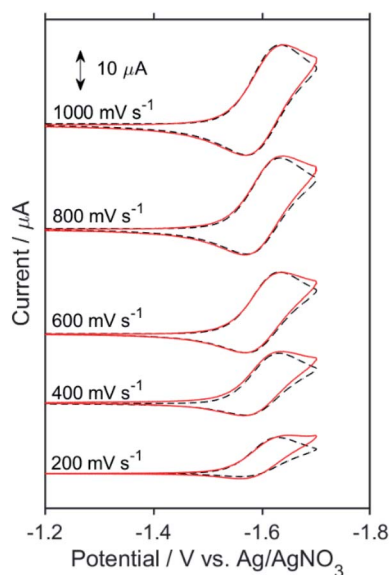

Fig. 10 Background subtracted CVs (red) and simulated CVs (black) of Re (1 mM); parameters: $E_1 = -1.60$ V ($k_s = 0.1$ cm s⁻¹), $k_c = 2.1$ s⁻¹, $D = 1.15 \times 10^{-6}$ cm² s⁻¹. WE: glassy carbon (diameter = 3 mm), RE: 0.01 mM Ag/AgNO₃, CE: Pt wire, supporting electrolyte: 0.1 M Et₄NBF₄ (0.1 M), scan rate: 200–1000 mV s⁻¹, $T = 298$ K.

metal complexes as catalysts.[5,8,29–31] This recombination mechanism is also supported by our previously reported linear relationships between CO formation rates and concentrations of the carbonate ester Re complexes in both photocatalytic and electrocatalytic CO_2 reduction reactions. This relationship is maintained even under a low concentration of CO_2 such as under Ar gas impregnated with only 0.5% CO_2.

Another mechanism is elimination of the carbonate ester ligand from the one-electron reduced species of the Re complex giving a five-coordinated 17-electron species, *i.e.*, $[Re^0(diimine)(CO)_3]$. Formation of a CO_2 coordinated complex $[Re^{II}(diimine)(CO)_3(CO_2)]$ from the five-coordinated 17-electron species has been proposed in some photochemical CO_2 reduction reactions using *fac*-$[Re^I(diimine)(CO)_3L]^{n+}$-type complexes as catalysts.[5,8] However, this elimination mechanism cannot explain the relationships between CO formation rates and concentrations of the carbonate ester Re complex as described above. In other words, this mechanism contradicts the previously reported high photocatalytic activity of the carbonate ester Re complexes even under a low concentration of CO_2.

The identification of the real mechanism is in progress in our laboratory.

Conclusions

Efficient photocatalytic reduction of CO_2 using **RuC2Re** as a photocatalyst and BIH as a sacrificial electron donor has been demonstrated to proceed in both DMSO–TEOA (5 : 1 v/v) and DMSO–THF–TEOA (5 : 5 : 2 v/v) solutions. The material balance of this photocatalytic reaction is shown in eqn (4), in which two molecules of CO_2 and one molecule of BIH make one molecule each of CO, HCO_3^-, and BI^+. The OERS **RuC2(Re)⁻**, as an essential intermediate in the photocatalytic reaction, is produced *via* two processes, namely, (1) the reductive quenching of the excited Ru unit followed by intramolecular electron transfer from the OERS of the Ru unit to the Re unit and (2) the reduction of **RuC2Re** in the ground state by $BI^•$, which is produced in process (1), followed by deprotonation. In **RuC2(Re)⁻**, the added electron is localised on the diimine ligand of the Re unit. Unimolecular reactions of **RuC2(Re)⁻** and its model mononuclear complex (**Re⁻**) proceed independently of the concentrations of CO_2 and the reduced and unreduced complexes in the reaction solution. The subsequent reaction of **RuC2(Re)⁻** was found to proceed with an observed first-order rate constant of 1.8 s^{-1} at 298 K, which is not dependent on either the concentrations of CO_2 or the OERS of **RuC2Re**. In the reaction of **Re⁻**, the activation energy, E_a, was estimated to be 46 kJ mol^{-1}. Although the structure of the "second" intermediate in the photocatalytic reduction remains unknown, it has already been elucidated that the second electron injection process involving the intermediate, which is necessary for the formation of CO and HCO_3^- (eqn (4)), proceeds in two ways, *i.e.*, *via* re-excitation of the Ru unit in the intermediate followed by reductive quenching and intramolecular electron transfer to the catalyst unit or *via* electron donation from reduced metal complexes, such as another intermediate made from the OERS

of **RuC2Re**, or $BI^•$, which was elucidated in a previous study using a **RuC2Re** derivative fixed on an Al_2O_3 surface.[32]

Experimental

General procedures

^{1}H and ^{13}C NMR spectra were recorded using a JEOL ECA400II (400 MHz) spectrometer. The residual protons of acetonitrile-d_3 and the ^{13}C of TEOA were used as internal standards in these measurements. FT-IR and UV-vis absorption spectra were recorded using JASCO FT-IR 6600 and JASCO V-565 spectrophotometers, respectively. CVs were recorded on an ALS/CHI620EX electrochemical analyser using DMSO–TEOA (5 : 1 v/v) solutions containing Et_4NBF_4 (0.1 M) as a supporting electrolyte, a glassy carbon disc working electrode (diameter = 3 mm, 1 mm or 33 μm), a Ag/AgNO₃ (0.01 M) reference electrode, and a Pt counter electrode. *iR* compensation was performed using the positive feedback method, which was implemented using the ALS/CHI620EX analyser.

Prior to its use in the measurements, DMSO was dried over 4 Å molecular sieves at room temperature, before being distilled in the presence of calcium hydride at reduced pressure. TEOA was distilled under reduced pressure (<133 Pa) prior to its use. After distillation, both solvents were stored under an Ar atmosphere. Et_4NBF_4 was dried under vacuum overnight at 100 °C prior to its use. All other reagents were of reagent grade quality and were used without further purification.

Synthesis

BIH and *fac*-$[(dmb)_2Ru(bpyC_2bpy)Re(CO)_3MeCN](PF_6)_2$ (**RuC2Re(MeCN)**), dmb = 4,4′-dimethyl-2,2′-bipyridine, bpyC₂-bpy = (4′-methyl-[2,2′-bipyridine]-4-yl)-CH_2CH_2-(4′-methyl-[2,2′-bipyridine]-4-yl)) were synthesised according to procedures published in the literature.[19,33,34] *fac*-$[Re(dmb)(CO)_3(CH_3CN)]^+$ (**Re(MeCN)**) was prepared according to the method for the synthesis of *fac*-$[Re(bpy)(CO)_3(CH_3CN)]^+$ described in the literature, except that *fac*-$Re(dmb)(CO)_3Br$ was used as a starting material.[1]

RuC2Re(MeCN) was dissolved in DMSO, and the resulting solution was kept at room temperature in the dark under an Ar atmosphere for 4 h for changing the MeCN ligand of all of the added Re complexes to the DMSO ligand because TEOA attacks the MeCN ligand of the Re complexes and an imino ester ligand is produced.[9] After this time, TEOA was added into the solution (DMSO : TEOA = 5 : 1 v/v), which was kept under an Ar atmosphere in the dark at room temperature for a period of more than 5 h. The resulting solution was bubbled with CO_2 to give a DMSO–TEOA (5 : 1 v/v) solution containing **RuC2Re**.

To synthesise a DMSO–TEOA (5 : 1 v/v) solution containing **Re**, the above method for **RuC2Re** was followed with **Re(MeCN)** used in place of **RuC2Re(MeCN)**.

Photocatalytic reactions

To carry out TON measurements, DMSO–THF–TEOA (5 : 5 : 2 v/v, 2.4 mL) or DMSO–TEOA (5 : 1 v/v, 2 mL) solutions containing **RuC2Re** (0.05 mM) and BIH (0.1 M) in 11 mL volume Pyrex test

tubes were purged with CO_2 for 20 min and then irradiated at 490–620 nm (λ_{max} = 530 nm) using an Iris-MG merry-go-round irradiation instrument equipped with a light-emitting diode (LED) light source (CELL System Co.). To carry out quantum yield measurements, in an 11 mL necked quartz cubic cell (path length: 1 cm), a CO_2-saturated DMSO–TEOA (5 : 1 v/v, 4 mL) solution containing **RuC2Re** (0.05 mM) and BIH (0.1 M) was irradiated at λ_{ex} = 480 nm (5.0×10^{-9} einstein s^{-1}) using a 300 W Xe lamp (Asahi Spectra MAX-303) equipped with a bandpass filter in a Shimadzu QYM-01 photoreaction quantum yield evaluation system. The sample temperature was kept at 25 °C ± 0.1 °C using an IWAKI CTS-134A temperature bath. The gaseous products, *i.e.*, CO and H_2, and formic acid in the solution were analysed *via* gas chromatography using a TCD (GL Sciences GC323) and a capillary electrophoresis system (Agilent Technologies 7100L), respectively.

Labelling experiments using $^{13}CO_2$

An NMR tube containing a DMSO-d_6 solution, TEOA (1.26 M), **RuC2Re** (0.14 mM), and BIH (0.1 M) was deaerated three times *via* a freeze–pump–thaw method, before adding $^{13}CO_2$ (537 mmHg). The ^1H and ^{13}C NMR spectra were measured before and after irradiation for 22 h using the same light source used in the photocatalytic reactions. The integration of the peaks using the NOE complete ^1H-decoupling method (EXMOD: nne, scan: 115, relaxation time: 400 s) was applied to determine the concentration of $H^{13}CO_3^-$, using the carbon in TEOA as an internal standard. The long relaxation time minimized the effects of NOE. The relaxation time should be 5 times longer than ^{13}C spin–lattice relaxation times (T_1) for integration.[35] Since T_1 of HCO_3^- was reported to be 10 s or less,[36] 400 s which we used as the delay time should be long enough for this measurement.

UV-vis absorption spectra during irradiation

In the case of **RuC2Re**, a CO_2-saturated DMSO–TEOA (5 : 1 v/v) solution containing **RuC2Re** (0.05 mM) and BIH (0.1 M) in an 11 mL necked quartz cubic cell (path length: 1 cm) was irradiated at λ_{ex} = 480 nm (2.6×10^{-8} einstein s^{-1}) using a 500 W Xe arc lamp equipped with a bandpass filter. In the case of **Ru**, an Ar-saturated DMSO–TEOA (5 : 1 v/v) solution containing **Ru** (0.05 mM) and BIH (0.1 M) in an 11 mL necked quartz cubic cell (path length: 1 cm) was irradiated at λ_{ex} = 480 nm (5.3×10^{-9} einstein s^{-1}) using a 500 W Xe arc lamp equipped with a band-pass filter. The temporal changes in the UV-vis absorption spectra were measured using a Photal MCPD-9800 photodiode array spectrometer (Ohtsuka Electronics Co., Ltd.). The sample temperature was kept at 25 °C ± 0.1 °C using an IWAKI CTS-134A temperature bath.

TR-vis spectroscopy

TR-vis spectroscopic measurements were performed using a picoTAS-ns-W2 picosecond transient absorption spectroscopy system (UNISOKU Co., Ltd.), operated using the RIPT method and a flow cell system (light pass length: 0.2 cm), as shown in Fig. S18.† A CO_2-saturated DMSO–TEOA (5 : 1 v/v) solution

containing the complex and BIH (0.1 M) was irradiated using Nd:YAG laser pulses at λ_{ex} = 532 nm (pulse width < 350 ps: 5 Hz).

TR-IR spectroscopy

TR-IR spectroscopic measurements were performed using a pump–probe method applying a subnanosecond laser for the pump pulse and a femtosecond Ti:sapphire laser for the probe pulse. The details of this procedure have been reported previously in the literature.[37–39] A tunable mid-infrared probe pulse was generated using a combination of optical parametric amplification and difference frequency generation (Light Conversion Ltd. Topas Prime, tunable range: 2500–12 000 nm; pulse energy: 40 μJ per pulse; bandwidth: 150 cm^{-1}) from a portion of the output of a femtosecond Ti:sapphire chirped-pulse amplifier (Spitfire Ace, Spectra-Physics; pulse duration: 120 fs; central wavelength: 800 nm; repetition rate: 1 kHz). The visible pump pulse was obtained by generating the second harmonic (532 nm) of a Nd:YVO$_4$ laser (InnoLas Laser Co. Picolo-AOT picosecond Nd:YVO$_4$ laser system; wavelength: 1064 nm; pulse duration: 0.6 ns) or the second harmonic (526.5 nm) of a laser (TECH-1053 basic diode-pumped Q-switched laser, Laser-export Co.; wavelength: 1053 nm; pulse duration: 10 ns) using an LBO crystal. The pump pulse was synchronised to the probe light *via* a function generator. The function generator reduced the repetition of a trigger pulse to 100 Hz. The fluence of the pump pulse was approximately 7 mJ cm^{-2}. The time control of the pump light and the probe light was performed by digitally controlling the delay using the function generator. The pump light and the probe light were focused to a FWHM of 220 and 200 μm, respectively. The probe light transmitted through the sample cell was guided to a poly-chromator (Horiba Co. TRIAX 190) coupled with a multichannel MCT array detector system (Infrared Systems Development FPAS-6416-D). The MCT detector was electronically gated at 100 Hz and was synchronised to the pulse generator, which prevents the detection of the unnecessary probe light. A homemade solution cell composed of BaF$_2$ window plates and a 0.5 mm Teflon spacer was filled with the sample solution. The samples were prepared as follows: CO_2 was bubbled into 20 mL of DMSO–TEOA (5 : 1 v/v) or DMSO–THF–TEOA (5 : 5 : 2 v/v) solutions containing the complex for 1 h. After the bubbling process was complete, BIH (448 mg, 0.1 M) was added to the solutions and additional CO_2 bubbling was conducted for approximately 15 min before carrying out the TR-IR measurements. CO_2 bubbling was continued during the measurements. In the case of the DMSO–THF–TEOA (5 : 5 : 2 v/v) solution, CO_2-saturated THF was added every 10 min to compensate for the concentration changes that arise because of the volatilisation of THF.

Quantum chemical calculations

Quantum chemical calculations based on DFT were performed using the *Gaussian 16* package.[40] Vibrational spectra were calculated after geometry optimisation of the ground and OER states. The LanL2DZ basis set and M06 functional were used to

compare the calculated and experimental TR-IR spectra. Time-dependent DFT (TDDFT) calculations of the excited states were also performed in DMSO solution using the general basis set of 6-311G++(d,p) used for geometry optimisation.

Digital simulation

The digital simulations of the CVs were performed by using an ALS/CHI620EX electrochemical analyser. Diffusion coefficients and $E_{1/2}$ values were determined from the CVs, assuming a heterogeneous rate constant of 0.1 cm s^{-1}. The rate constant of the chemical reaction (k_c) was determined by fitting the background subtracted CVs measured at various scan speeds.

Data availability

All the data supporting this article have been included in the main text and the supplementary material.

Author contributions

K. Kamogawa: most of experiments, writing of manuscript. Y. Shimoda: TR-IR measurements, DFT calculations. K. Miyata: TR-IR measurements, DFT calculations. K. Onda: TR-IR measurements, DFT calculations, writting of the TR-IR part. Y. Yamazaki: discussion. Y. Tamaki: supervision of experiments, discussion. O. Ishitani: conceptualization, funding acquisition, and supervision; writing, review, and editing of manuscript.

Conflicts of interest

There are no conflicts to declare.

Acknowledgements

Notes and references

1 (a) J. Hawecker, J.-M. Lehn and R. Ziessel, *J. Chem. Soc., Chem. Commun.*, 1983, 536–538; (b) J. Hawecker, J.-M. Lhen and R. Ziessel, *Helv. Chim. Acta*, 1986, **69**, 1990–2012.

2 (a) H. Hori, F. P. A. Johnson, K. Koike, O. Ishitani and T. Ibusuki, *J. Photochem. Photobiol., A*, 1996, **96**, 171–174; (b) H. Takeda, K. Koike, H. Inoue and O. Ishitani, *J. Am. Chem. Soc.*, 2008, **130**, 2023–2031.

3 (a) T. Morimoto, C. Nishiura, M. Tanaka, J. Rohacova, Y. Nakagawa, Y. Funada, K. Koike, Y. Yamamoto, S. Shishido, T. Kojima, T. Saeki, T. Ozeki and O. Ishitani, *J. Am. Chem. Soc.*, 2013, **135**, 13266–13269; (b) J. Rohacova and O. Ishitani, *Chem. Sci.*, 2016, **7**, 6728–6739.

4 (a) Y. Kuramochi, O. Ishitani and H. Ishida, *Coord. Chem. Rev.*, 2018, **373**, 333–356; (b) Y. Tamaki, H. Takeda and O. Ishitani, in *Molecular Technology*, ed. H. Yamamoto and T. Kato, Wiley-VCH Verlag GmbH & Co. KGaA, 2019, vol. 1, pp. 209–249.

5 Y. Kou, Y. Nabetani, D. Masui, T. Shimada, S. Takagi, H. Tachibana and H. Inoue, *J. Am. Chem. Soc.*, 2014, **136**, 6021–6030.

6 Y. Hayashi, S. Kita, B. S. Brunschwig and E. Fujita, *J. Am. Chem. Soc.*, 2003, **125**, 11976–11987.

7 J. Agarwal, E. Fujita, H. F. Schaefer and J. T. Muckerman, *J. Am. Chem. Soc.*, 2012, **134**, 5180–5186.

8 T. W. Schneider, M. Z. Ertem and J. T. Muckerman, *ACS Catal.*, 2016, **6**, 5473–5481.

9 T. Morimoto, T. Nakajima, S. Sawa, R. Nakanishi, D. Imori and O. Ishitani, *J. Am. Chem. Soc.*, 2013, **135**, 16825–16828.

10 T. Nakajima, Y. Tamaki, K. Ueno, E. Kato, T. Nishikawa, K. Ohkubo, Y. Yamazaki, T. Morimoto and O. Ishitani, *J. Am. Chem. Soc.*, 2016, **138**, 13818–13821.

11 H. Kumagai, T. Nishikawa, H. Koizumi, T. Yatsu, G. Sahara, Y. Yamazaki, Y. Tamaki and O. Ishitani, *Chem. Sci.*, 2019, **10**, 1597–1606.

12 B. Gholamkhass, H. Mametsuka, K. Koike, T. Tnabe, M. Furue and O. Ishitani, *Inorg. Chem.*, 2005, **44**, 2326–2336.

13 Y. Tamaki, K. Koike, T. Morimoto, Y. Yamazaki and O. Ishitani, *Inorg. Chem.*, 2013, **52**, 11902–11909.

14 Y. Kuramochi and O. Ishitani, *Inorg. Chem.*, 2016, **55**, 5702–5709.

15 Y. Tamaki and O. Ishitani, *ACS Catal.*, 2017, **7**, 3394–3409.

16 Y. Tamaki, K. Koike, T. Morimoto and O. Ishitani, *J. Catal.*, 2013, **304**, 22–28.

17 A. M. Cancelliere, F. Puntoriero, S. Serroni, S. Campagna, Y. Tamaki, D. Saito and O. Ishitani, *Chem. Sci.*, 2020, **11**, 1556–1563.

18 E. Kato, H. Takeda, K. Koike, K. Ohkubo and O. Ishitani, *Chem. Sci.*, 2015, **6**, 3003–3012.

19 K. Ohkubo, Y. Yamazaki, T. Nakashima, Y. Tamaki, K. Koike and O. Ishitani, *J. Catal.*, 2016, **343**, 278–289.

20 (a) H. Kumagai, G. Sahara, M. Higashi, R. Abe and O. Ishitani, *Chem. Sci.*, 2017, **8**, 4242–4249; (b) G. Sahara, H. Kumagai, K. Maeda, N. Kaeffer, V. Artero, M. Higashi, R. Abe and O. Ishitani, *J. Am. Chem. Soc.*, 2016, **138**, 14152–14158.

21 Y. Ueda, H. Takeda, T. Yui, K. Koike, Y. Goto, S. Inagaki and O. Ishitani, *ChemSusChem*, 2015, **8**, 439–442.

22 *NIST Physical Measurement Laboratory, http://www.nist.gov/pml/data/comp.cfm.

23 The FT-IR cell with $d = 0.2$ mm was too thin to allow the DMSO–TEOA (5 : 1 v/v) solution to flow because of its high viscosity. Although we could solve this problem by increasing the thickness of the flow IR cell to $d = 0.5$ mm and all of the stretching bands of the CO ligands were measurable even when using this thick cell, the absorbance of the solvent was too high for the C=O stretching band of the carbonate ester ligand to be measured.

24 S. Sato, Y. Matubara, K. Koike, M. Falkenström, T. Katayama, Y. Ishibashi, H. Miyasaka, S. Taniguchi, H. Chosrowjan, N. Mataga, N. Fukuzawa, S. Koshihara, K. Onda and O. Ishitani, *Chem.–Eur. J.*, 2012, **18**, 15722–15734.

25 K. Koike, D. C. Grills, Y. Tamaki, E. Fujita, K. Ohkubo, Y. Yamazaki, M. Saigo, T. Mukuta, K. Onda and O. Ishitani, *Chem. Sci.*, 2018, **9**, 2961–2974.

26 Y. Yamazaki, K. Ohkubo, D. Saito, T. Yatsu, Y. Tamaki, S. Tanaka, K. Koike, K. Onda and O. Ishitani, *Inorg. Chem.*, 2019, **58**, 11480–11492.

27 T. Nakagawa, K. Okamoto, H. Hanada and R. Katoh, *Opt. Lett.*, 2016, **41**, 1498–1501.

28 S. Sato, K. Koike, H. Inoue and O. Ishitani, *Photochem. Photobiol. Sci.*, 2007, **6**, 454–461.

29 M. D. Sampson, J. D. Froehlich, J. M. Smieja, E. E. Benson, I. D. Sharp and C. P. Kubiak, *Energy Environ. Sci.*, 2013, **6**, 3748–3755.

30 J. A. Keith, K. A. Grice, C. P. Kubiak and E. A. Carter, *J. Am. Chem. Soc.*, 2013, **135**, 15823–15829.

31 H. Ishida, K. Tanaka and T. Tanaka, *Organometallics*, 1987, **6**, 181–186.

32 D. Saito, Y. Yamazaki, Y. Tamaki and O. Ishitani, *J. Am. Chem. Soc.*, 2020, **142**, 19249–19258.

33 E. Hasegawa, T. Seida, N. Chiba, T. Takahashi and H. Ikeda, *J. Org. Chem.*, 2005, **70**, 9632–9635.

34 X.-Q. Zhu, M.-T. Zhang, A. Yu, C.-H. Wang and J.-P. Cheng, *J. Am. Chem. Soc.*, 2008, **130**, 2501–2516.

35 P. Giraudeau, J. L. Wang and E. Baguet, *C. R. Chim.*, 2006, **9**, 525–529.

36 H. Yamada, F. A. Chowdhury, K. Goto and T. Higashii, *Int. J. Greenhouse Gas Control*, 2013, **17**, 99–105.

37 T. Mukuta, N. Fukazawa, K. Murata, A. Inagaki, M. Akita, S. Tanaka, S. Koshihara and K. Onda, *Inorg. Chem.*, 2014, **53**, 2481–2490.

38 T. Mukuta, S. Tanaka, A. Inagaki, S. Koshihara and K. Onda, *ChemistrySelect*, 2016, **1**, 2802–2807.

39 T. Mukuta, P. Simpson, J. G. Vaughan, B. W. Skelton, S. Stagni, M. Massi, K. Koike, O. Ishitani and K. Onda, *Inorg. Chem.*, 2017, **56**, 3404–3413.

40 M. J. Frisch, G. W. Trucks, H. B. Schlegel, G. E. Scuseria, M. A. Robb, J. R. Cheeseman, G. Scalmani, V. Barone, G. A. Petersson, H. Nakatsuji, X. Li, M. Caricato, A. V. Marenich, J. Bloino, B. G. Janesko, R. Gomperts, B. Mennucci, H. P. Hratchian, J. V. Ortiz, A. F. Izmaylov, J. L. Sonnenberg, D. Williams-Young, F. Ding, F. Lipparini, F. Egidi, J. Goings, B. Peng, A. Petrone, T. Henderson, D. Ranasinghe, V. G. Zakrzewski, J. Gao, N. Rega, G. Zheng, W. Liang, M. Hada, M. Ehara, K. Toyota, R. Fukuda, J. Hasegawa, M. Ishida, T. Nakajima, Y. Honda, O. Kitao, H. Nakai, T. Vreven, K. Throssell, J. A. Montgomery Jr, J. E. Peralta, F. Ogliaro, M. J. Bearpark, J. J. Heyd, E. N. Brothers, K. N. Kudin, V. N. Staroverov, T. A. Keith, R. Kobayashi, J. Normand, K. Raghavachari, A. P. Rendell, J. C. Burant, S. S. Iyengar, J. Tomasi, M. Cossi, J. M. Millam, M. Klene, C. Adamo, R. Cammi, J. W. Ochterski, R. L. Martin, K. Morokuma, O. Farkas, J. B. Foresman, and D. J. Fox, *Gaussian 16, Revision A.03*, Gaussian, Inc., Wallingford CT, 2016.